A geophysical index to map alteration, permeability, and mechanical properties within volcanoes. Application to the soft volcanic rocks from Whakaari/White Island (New Zealand)

André Revil, Antoine Coperey, Michael J Heap, Lucille Carbillet

Journal of Volcanology and Geothermal Research 401 (2020) 106945

Contents lists available at ScienceDirect

Journal of Volcanology and Geothermal Research

journal homepage: www.elsevier.com/locate/jvolgeores

A geophysical index to map alteration, permeability, and mechanical properties within volcanoes. Application to the soft volcanic rocks from Whakaari/White Island (New Zealand)

André Revil [a,*], Antoine Coperey [b], Michael J. Heap [c], Lucille Carbillet [c]

[a] Université Grenoble Alpes, USMB, CNRS, EDYTEM, 73000 Chambéry, France
[b] Univ. Grenoble Alpes, Univ. Savoie Mont Blanc, CNRS, IRD, IFSTTAR, ISTerre, 38000 Grenoble, France
[c] Géophysique Expérimentale, Institut de Physique de Globe de Strasbourg, UMR 7516 CNRS, Université de Strasbourg/EOST, Strasbourg cedex, France

ARTICLE INFO

Article history:
Received 30 March 2020
Received in revised form 25 May 2020
Accepted 27 May 2020
Available online 30 May 2020

Keywords:
Cation exchange capacity
Alteration
Compressive strength
Permeability

ABSTRACT

The alteration of soft volcanic rocks (i.e., characterized by a low uniaxial compressive strength <35 MPa) can change their permeability and mechanical strength. We built an alteration indicator based on porosity and cation exchange capacity (CEC) to connect the degree of alteration of soft volcanic rocks to their permeability and uniaxial compressive strength. The proposed empirical petrophysical relationships are validated using a dataset of 62 samples from Whakaari/White Island (New Zealand). Since porosity and CEC can be imaged with induced polarization, this geophysical method can be used to map permeability and mechanical properties for near-surface formations at active volcanoes worldwide.

1. Introduction

The stability of volcanic edifices denotes a significant geohazard (e.g., McGuire, 1996; Voight, 2000) which rests, in part, on the mechanical properties of the edifice-forming rocks. Hydrothermal alteration, common to many active volcanoes worldwide (Zimbelman et al., 2005; Rosas-Carbajal et al., 2016), can modify the physical properties of volcanic rocks (e.g., Pola et al., 2012; Wyering et al., 2014; Frolova et al., 2014; Mordensky et al., 2019), which can lead to an increased risk of edifice instability (e.g., Watters et al., 2000; Finn et al., 2001; Reid et al., 2001; John et al., 2008; Peruzzetto et al., 2019). The permeability of volcanic rocks, a metric considered important in dictating the volcanic character—effusive or explosive—of a volcano (e.g., Eichelberger et al., 1986; Mueller et al., 2008; Collinson and Neuberg, 2012; Farquharson et al., 2017; Cassidy et al., 2018), can also be influenced by hydrothermal alteration (e.g., Sruoga et al., 2004; Heap et al., 2017; Mordensky et al., 2018; Heap et al., 2019, 2020). Since alteration also modifies the cation exchange capacity (CEC) of volcanic rocks (e.g., Revil et al., 2017a, 2017b; Revil et al., 2019), it is therefore of interest to develop an alteration index based on both porosity and CEC, both of which can be imaged using geophysical methods such as induced polarization (Ghorbani et al., 2018). If empirical relationships between rock physical properties (such as uniaxial compressive strength and permeability) and the CEC and porosity can be established in the laboratory, induced polarization could therefore be used to map out, for example, the permeability and strength structure of the volcano (see recently Revil et al., 2019, for a preliminary step in this direction).

In this paper, we first develop an alteration indicator based on porosity and the CEC. We then use a collection of 62 hydrothermally altered rock samples from Whakaari/White Island (New Zealand), hereafter referred to as Whakaari, to see if we can predict their permeability and uniaxial compressive strength using our proposed alteration index.

2. Previous results

Revil et al. (2019) derived a petrophysical model connecting the electrical conductivity and the normalized chargeability of volcanic rocks to the CEC and porosity of the material. These authors were able to use these petrophysical relationships to image porosity and CEC over an active geothermal field at Krafla volcano in Iceland. We briefly summarize these relationships in this section. First of all, the CEC (in meq/100 g, 1 meq/100 g = 963.20 C.kg^{-1}) denotes the sorbed charges on the surface of the minerals (in the electrical double layer) per unit mass of grains and is proportional to the specific surface area (surface area of grains per unit mass of grains) (Moore et al., 1998). The CEC can be also normalized per unit pore volume of rock. The total volumetric charge density, Q_V, (expressed in C m^{-3}) can be written as a function of the cation exchange capacity CEC expressed in C kg^{-1} (e.g., Waxman and Smits, 1968)

* Corresponding author.
E-mail addresses: andre.revil@univ-smb.fr (A. Revil), heap@unistra.fr (M.J. Heap), lcarbillet@unistra.fr (L. Carbillet).

https://doi.org/10.1016/j.jvolgeores.2020.106945
0377-0273/

$$Q_V = \rho_g \left(\frac{1-\phi}{\phi}\right) \mathrm{CEC}, \quad (1)$$

where ρ_g denotes the mass density of the grains (typically ~2600--3000 kg m^{-3}; e.g., Okay et al., 2014) and ϕ the connected porosity. The conductivity, σ_∞, and normalized chargeability, M_n, are given by (Revil et al., 2019)

$$\sigma_\infty = \frac{1}{F}[\sigma_w + mBQ_V] \quad (2)$$

$$M_n = \frac{m}{F}\lambda Q_V, \quad (3)$$

where σ_w denotes the pore water conductivity (in S m^{-1}), B and λ (in m^{2}s^{-1} V^{-1}) are two effective mobilities for the surface and the normalized chargeability, respectively (see Ghorbani et al., 2018, for specific values). The connection between the dimensionless formation factor, F, and the porosity, ϕ, is called Archie's law, $F = \phi^{-m}$ where m (dimensionless) is the porosity exponent (sometimes called the cementation exponent or first Archie's exponent). The fit of this relationship for a large set of experimental data for volcanic rocks is shown in Fig. 1, with the mean value of $m = 2.57 \pm 0.10$. Typically, m is between 2 and 3 for volcanic rocks (Revil et al., 2017a, 2017b). The relationship between the normalized chargeability and the excess of charge density, Q_V, is shown in Fig. 2 in which the value of λ is determined. Eqs. (2) and (3) represent what is needed to determine the porosity and Q_V fields for a volcanic area. In the next section, we attempt to form a relationship between Q_V and the permeability and mechanical properties (i.e., strength) of volcanic rocks.

3. Permeability and uniaxial compressive strength

Sen et al. (1990) proposed the following relationship between the formation factor, the excess of charge per unit pore volume, and the permeability, k

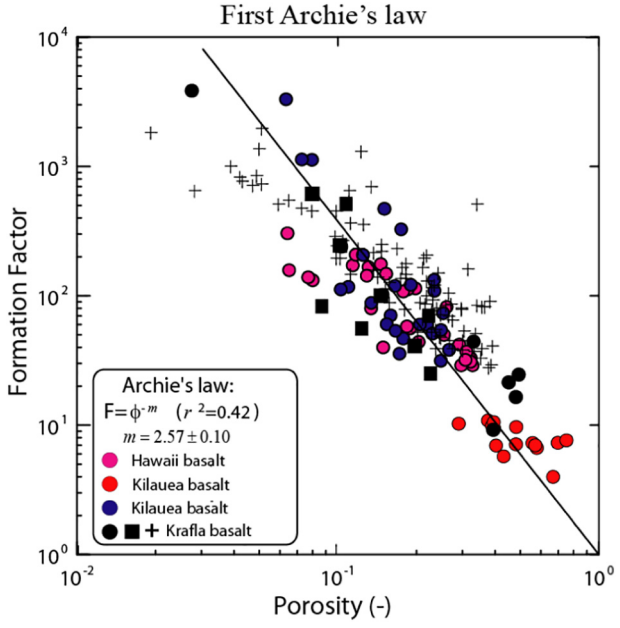

Fig. 1. Electrical formation factor as a function of connected porosity (modified from Revil et al., 2019). We fit the complete data set with Archie's law $F = \phi^{-m}$ (Archie, 1942) where the fitted cementation exponent is $m = 2.57 \pm 0.10$ (dimensionless). This figure provides a relationship for volcanic rocks between the (intrinsic) formation factor and the (connected) porosity. This relationship is of prime importance to interpret conductivity and induced polarization data in the field in terms of inverting the porosity and the cation exchange capacity.

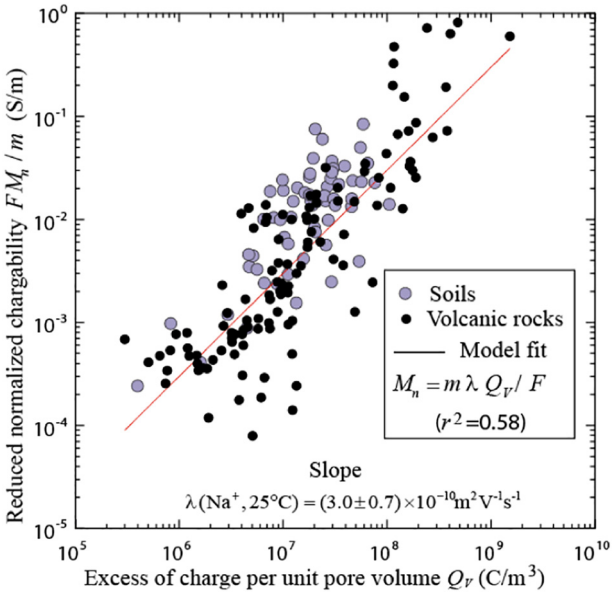

Fig. 2. Reduced normalized chargeability as a function of the excess of charge per unit pore volume determined from the porosity and the cation exchange capacity. The trend is fitted according to a linear trend passing through the origin of the coordinates (modified from Revil et al., 2019) and is here applied only to the volcanic rocks. This figure provides a universal relationship for volcanic rocks between the (reduced) normalized chargeability and the excess of charge per unit pore volume. This relationship is of prime importance to interpret conductivity and induced polarization data in the field in terms of inverting the porosity and the cation exchange capacity.

$$k = k_0 (1/FQ_V)^c, \quad (4)$$

where k_0 and c are two fitting parameters (with k in m^2, $1/FQ_V$ in m^3 C^{-1}). Eq. (2) extends an equation proposed by Goode and Sen (1988) in which the permeability can be predicted from Q_V. Similarly, we propose that the uniaxial compressive strength of a sample (E in MPa) can be related to the same alteration indicator FQ_V as

$$E = a \log_{10}(1/FQ_V) + b, \quad (5)$$

where a and b are empirical constants. Eq. (5) has no physical basis and should be considered in this paper as a purely empirical construct used to fit the data. In this paper, we aim to test the effectiveness of Eqs. (4) and (5) for volcanic rocks and to determine the empirical parameters k_0, a, b, and c for a broad collection of volcanic rocks.

4. Laboratory experiments

The samples used in this study are from Whakaari, an active andesitic-dacitic stratovolcano located at the northernmost tip of the Taupō Volcanic Zone (New Zealand) (Fig. 3). Whakaari hosts a hydrothermal system (e.g., Giggenbach et al., 2003), and the hydrothermal alteration of edifice-forming and conduit rocks has been shown to influence their mechanical behaviour (Heap et al., 2015), permeability (Heap et al., 2017; Kennedy et al., 2020), and fragmentation threshold (Mayer et al., 2016). Geomorphic evidence also points to major flank failures involving weak hydrothermally altered rocks (Moon et al., 2009).

A total of 62 cylindrical core samples (20 mm in diameter and nominally 40 mm in length) were used for this study (Fig. 3). These samples were cored from blocks collected from the accessible scree adjacent to the crater wall and comprise tuffs, lavas, and lava breccias (sample collection sites are indicated on Fig. 4). The connected porosity (measured using the connected volume given by a helium pycnometer and the sample dimensions) and permeability (measured using a benchtop gas permeameter; Heap and Kennedy, 2016) of these samples were

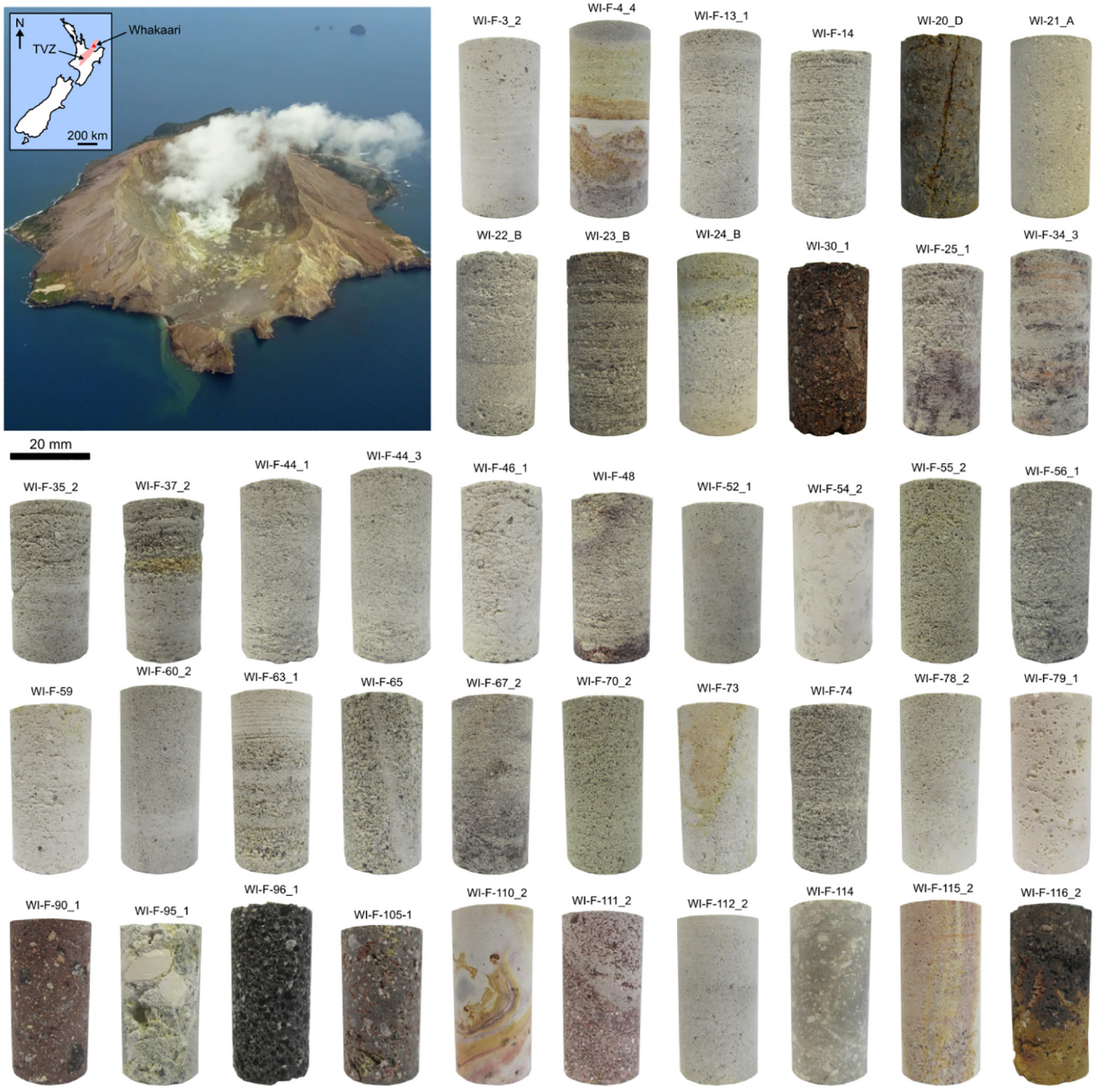

Fig. 3. Photographs of the experimental samples (20 mm in diameter and nominally 40 mm in length) from Whakaari (New Zealand) (photographs of duplicate cores, cored from the same block, are omitted). Top left shows a photograph of Whakaari; inset shows a map of New Zealand with the locations of the Taupō Volcanic Zone (TVZ) and Whakaari indicated.

measured in a previous contribution (Heap et al., 2017; Table 1). The samples were first dried in a vacuum-oven for at least 48 h. They were then deformed uniaxially at a constant strain rate of 10^{-5} s^{-1} until macroscopic failure. During deformation, a load cell and a linear variable differential transducer measured the axial load and axial displacement, respectively, which were then converted to axial stress and axial strain using the sample dimensions. A lubricating wax was applied to the end-faces of the samples to avoid problems with friction between the sample and piston. All experiments were performed at room temperature. The broken samples were then powdered by hand using a pestle and mortar to a particle size ≪2 mm.

The CEC can be taken as a proxy of the clay content of a material at constant clay and zeolite mineralogy (Revil et al., 2017a, 2017b) and in some cases as an alteration indicator for volcanic rocks (Ghorbani et al., 2018; Revil et al., 2019). To measure the CEC of the powdered samples in the laboratory, we used the pH-free Hexamine cobalt chloride method and spectrophotometric titration (Ciesielski et al., 1997). We adapted the protocol described in Aran et al. (2008) for volcanic rocks. The samples were reduced to a fine powder, which was dried for 24 h at 80 °C. In a centrifuge tube, about 4 g of the dry powder was reacted with 40 ml of cobalt chloride hexamine at 0.05 N for one day. In our case, a first set of CEC measurements was performed with 2 g of powder, as prescribed by Aran et al. (2008), but the amount of adsorbed cobalt was below the detection threshold of the spectrophotometer (Bibby Scientific™ Jenway™ 6320D). Next, the solution-powder mix was centrifuged for 10 min and the supernatant was filtered for the measurement of absorbance by the spectrophotometer. Hexamine cobalt chloride solution has an orange colour with a maximal absorbance at 472 nm. The solution becomes clearer as more cobalt ions are adsorbed.

The CEC was calculated by taking into account the mass of powder, the volume of solution, and the difference in absorbance between the raw solution and the supernatant, see Aran et al. (2008) for details. In order to check the stability of the absorbance measurement, the absorption of demineralized water was regularly performed and, at the end of the sample set, some supernatants were measured again. In addition, in order to quantify our errors, the CEC of 10 samples was re-measured on new powder (see Table 1). The standard deviations were found to be between 0.03

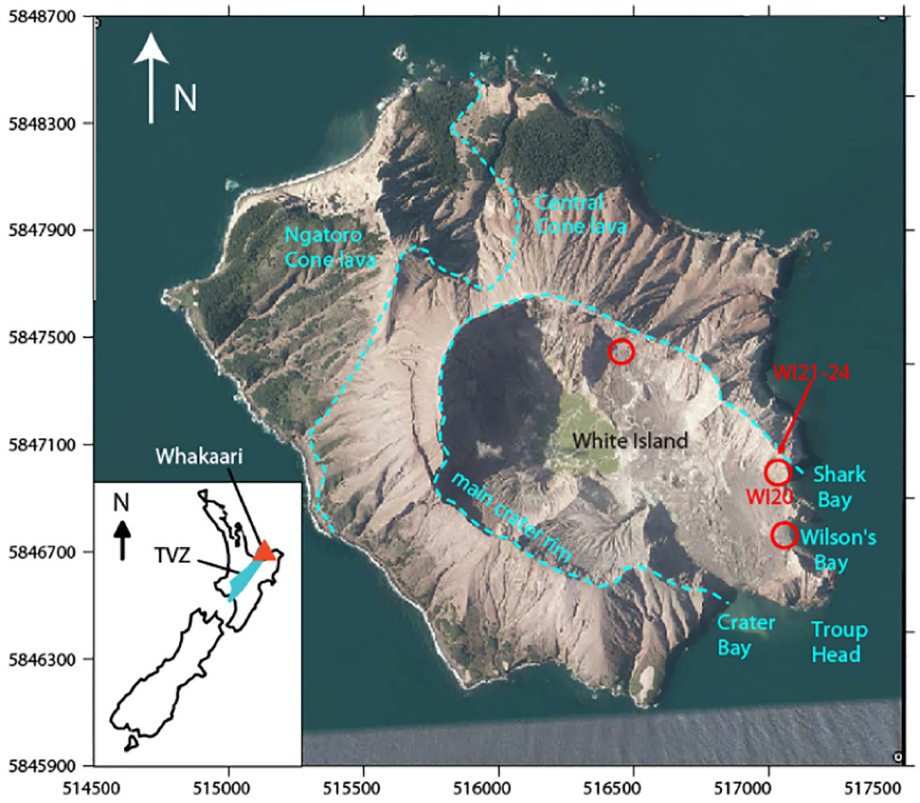

Fig. 4. Map of Whakaari/White Island volcano (Bay of Plenty, New Zealand) showing the locations of the sample collection sites (indicated by the red open circles). The inset shows a map of New Zealand showing the location of the Taupō Volcanic Zone (TVZ, blue area) and Whakaari volcano (red triangle). Figure modified from Heap et al. (2017) (coordinate system, UTM WGS84, 60M). (For interpretation of the references to colour in this figure legend, the reader is referred to the web version of this article.)

and 0.31 meq/100 g, except for sample WI 37 (which is characterized by a standard deviation of 1.35 meq/100 g with an average value of 5 meq/100 g). Just after the measurement of absorbance, the temperature and the pH of the supernatant were also recorded and are reported in Table 1. In our study, the porosity are transformed to formation factors by using Archie's law with $m = 2.57$ as shown in Fig. 1.

5. Results and discussion

As shown in Fig. 5, the porosity and the cation exchange capacity are two independent parameters that are therefore complementary in characterizing volcanic rocks. In Fig. 6, we plot permeability and uniaxial compressive strength as a function of connected porosity (data available

Table 1
Relevant petrophysical properties of 22 core samples from Whakaari volcano (White Island) in New Zealand and used for the measured electrical properties. The quantity ρ_g denotes the grain density (kg m^{-3}), ϕ the connected porosity (dimensionless), F the electrical (intrinsic) formation factor (dimensionless), CEC (expressed in meq/100 g) denotes the cation exchange capacity, σ'' (in S m^{-1}) denotes the quadrature conductivity at 1 Hz, S_{sp} corresponds to the specific surface area measured with the BET technique, and k is the permeability (measured at a confining pressure of 1 MPa; data from Heap et al., 2017). The formation factor is the intrinsic formation factor F obtained by fitting a conductivity law $\sigma = \sigma_w / F + \sigma_S$ (σ is the conductivity of the rock, σ_w is the conductivity of the pore water, σ_S is the surface conductivity) using a dataset obtained at different salinities.

Sample	ϕ (−)	ρ_g (kg m^{-3})	F (−)	CEC (meq/100 g)	S_{sp} (m^2/g)	σ_S (10^{-4} S m^{-1})	σ'' (10^{-5} S m^{-1})	k (m^2)	Type
3	0.555	2145	7	0.686	–	16.8	1.5	1.00×10^{-16}	Lithified ash tuff
4	0.399	2182	66	0.767	–	13.7	0.3	1.94×10^{-15}	Lithified ash tuff
34	0.500	2160	8	0.812	–	14.3	1.3	3.01×10^{-13}	Lithified ash tuff
55	0.437	2235	9	0.341	–	4.8	0.8	9.42×10^{-13}	Lithified ash tuff
67	0.496	2152	8	0.469	–	12.0	0.6	4.98×10^{-13}	Lithified ash tuff
70	0.461	2231	8	1.152	–	13.6	0.2	1.52×10^{-12}	Lithified ash tuff
78	0.436	2204	28	0.514	–	25.8	1.1	3.61×10^{-15}	Lithified ash tuff
91	0.308	2242	16	0.810	–	15.9	1.1	1.65×10^{-12}	Lava breccia
99	0.129	2084	190	0.811	–	1.4	0.1	2.79×10^{-14}	Lava breccia
102	0.197	2240	19	0.426	–	76.1	0.4	5.55×10^{-13}	Lava breccia
105	0.269	2223	190	0.342	–	5.1	0.2	1.28×10^{-14}	Lava breccia
107	0.261	2320	36	0.727	–	15.0	1.5	6.69×10^{-13}	Lava breccia
110	0.374	2410	25	0.727	–	31.9	0.6	8.62×10^{-18}	Lithified ash tuff
111	0.436	2255	10	0.684	–	5.5	0.6	2.90×10^{-13}	Lava breccia
112	0.357	2290	15	1.320	–	12.7	1.1	2.38×10^{-16}	Lithified ash tuff
115	0.484	2167	13	0.643	–	14.3	1.4	4.33×10^{-15}	Lithified ash tuff
116	0.405	3171	26	1.409	–	12.6	0.7	2.51×10^{-13}	Lava breccia
W120	0.059	2686	1027	2.818	15.8	24.2	1.8	7.05×10^{-17}	Andesitic lava
W121	0.358	2240	23	0.812	4.4	4.7	0.8	1.27×10^{-16}	Lithified ash tuff
W122	0.448	2022	15	0.215	3.9	13.9	1.2	3.14×10^{-15}	Lithified ash tuff
W123	0.420	2244	13	1.890	11.4	19.3	3.6	1.21×10^{-15}	Lithified ash tuff
W124	0.466	2115	8	0.428	4.6	11.9	1.5	3.08×10^{-13}	Lithified ash tuff

in Table 2). It is typical for permeability to increase as a function of increasing porosity for volcanic rocks (e.g., Saar and Manga, 1999; Mueller et al., 2005; Farquharson et al., 2015; Wadsworth et al., 2016). The permeability of samples of tuffs, lavas, and breccias from Whakaari also show an increasing trend with increasing porosity (Heap et al., 2017; Kennedy et al., 2020). Heap et al. (2017) highlighted that, due to the extreme variability of these samples in terms of texture, microstructure, and alteration, trends are only observable for very large datasets. There is no discernible trend in the permeability-porosity data presented here (Fig. 6), a subset of the data presented in Heap et al. (2017), because of the variability in rock type (tuff, lava, and breccia) and the variability (terms of texture, microstructure, and alteration) between samples of the same rock type (see Fig. 3 and thin section images shown in Heap et al., 2015, 2017). Heap et al. (2017) concluded that the permeability of the tuff samples, the most abundant rock type in our dataset, decreases with increasing pore-filling alteration (e.g., the precipitation of alunite).

Fig. 6 also shows that, in general, uniaxial compressive strength decreases as a function of increasing porosity (data unique to this study; Table 2), in agreement with previous studies on the strength of volcanic rocks (e.g., Al-Harthi et al., 1999; Heap et al., 2014; Wyering et al., 2014; Schaefer et al., 2015; Coats et al., 2018; Mordensky et al., 2018). In general, the strongest samples were lavas (WI_20_D and WI_F_114 had a strength of 71.7 and 111.9 MPa, respectively) and the weakest samples were tuffs, the strength of which varied from a couple of tens of MPa to a couple of MPa (Table 2; Fig. 3). We conclude, analogous to the conclusions drawn by Heap et al. (2017), that the strength of the tuff samples increases with increasing alteration due to pore-filling alteration. Previous studies have also found the strength of volcanic rocks increases with increasing pore-filling hydrothermal alteration (e.g., Mordensky et al., 2018; Heap et al., 2020).

Our permeability and uniaxial compressive strength data (Fig. 6; Table 2) represent ideal data with which to test Eqs. (2) and (3) due to the scatter as a result of their variability in terms of texture, microstructure, and alteration (see Fig. 3). The permeability and uniaxial compressive strength are shown as a function of the alteration indicator in Figs. 7 and 8, respectively. Fig. 7 is consistent with the data reported in Revil et al. (2019) for soils. Fig. 7 shows that the alteration indicator predicts the permeability fairly well within the range 10^{-16} to 10^{-12} m^2. It would be interesting to extend the trend in the future by adding more altered rocks rich in smectite and characterized by very low permeabilities (i.e., below 10^{-16} m^2). Fig. 8 shows that the uniaxial compressive strength can be predicted from the porosity and the water content with confidence (over a wide range of strengths, from a couple of MPa to >100 MPa). The values of the empirical parameters defined above are given by $k_0 = 1.46 \times 10^6$ ($\log k_0 = 6.17 \pm 2.35$), $c = 2.88 \pm 0.34$, $a = -20 \pm 2$, $b = -127 \pm 15$, for our collection of volcanic rocks.

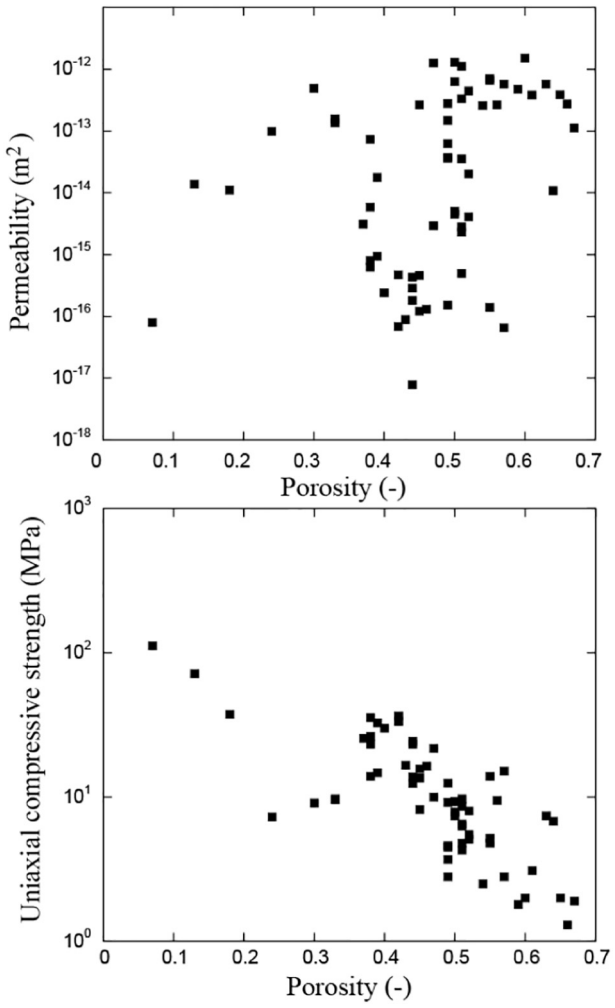

Fig. 6. Permeability and uniaxial compressive strength as a function of connected porosity for the rock samples from Whakaari (New Zealand). For the first plot we observe no correlation between the two parameters while we observe a weak correlation between the uniaxial compressive strength and the porosity in the second plot (see text for details).

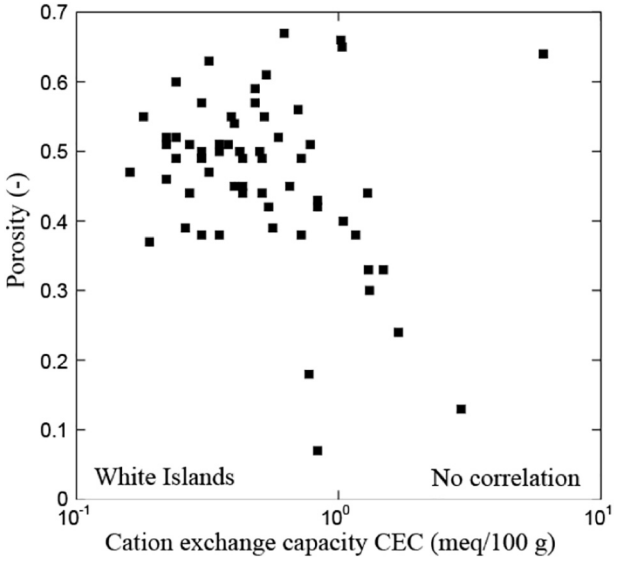

Fig. 5. Porosity as a function of cation exchange capacity for the samples from Whakaari (New Zealand). This figure shows that the two parameters are independent from each other and are therefore complementary in characterizing volcanic rocks.

These results are far-reaching in the realm of hydrogeophysics applied to volcanology. Indeed, a geophysical method such as induced polarization can be used to map porosity and water content. Induced polarization extends the electrical conductivity/resistivity method (Waxman and Smits, 1968) to include the low frequency polarization of rocks associated with their ability to store reversibly electrical charges under the influence of a primary electrical field/current (Vinegar and Waxman, 1984). A model based on the polarization of the electrical double layer coating the surface of the grains, called the dynamic Stern layer model (Revil et al., 2019, and references therein), has been previously applied to volcanic rocks (Revil et al., 2017a, 2017b, 2019). This model can be used to map in 3D the porosity and CEC in the field using either galvanometric (such as time domain induced polarization) or induction-based techniques (such as the airborne time-domain electromagnetic method). Therefore, Eqs. (2) and (3) can be used in conjunction with this method to map the 3D permeability and strength structure of active volcanoes worldwide. These

Table 2
Relevant petrophysical parameters of the samples from Whakaari volcano (White Island) in New Zealand. The CEC values with * correspond to an average value (measurements made on two batches of powder from the samples). Just after the measurement of the absorbance, the temperature and the pH of Hexamine cobalt chloride supernatant were measured. The neutral solution of Hexamine cobalt (III) chloride has a pH of 6.55 at 20.1 °C. The samples are mostly tuffs and a few lavas and lava breccias called WI 30 (Fig. 3). UCS – uniaxial compressive strength.

Sample	Dry bulk density (g/cm^3)	Connected porosity (−)	Permeability (m^2)	UCS (MPa)	CEC (meq/100 g)	pH of supernatant	Temperature of supernatant (°C)
WI F 3_2	0.980	0.57	6.53×10^{-17}	15.1	0.30	5.55	21.2
WI F 4_2	1.306	0.45	4.62×10^{-16}	15.7	0.40	3.51	21.4
WI F 4_3	1.325	0.44	7.88×10^{-18}	13.8	0.51	3.68	18.3
WI F 4_4	1.335	0.43	8.89×10^{-17}	16.6	0.83	3.79	18.3
WI F 13_1	1.134	0.51	4.96×10^{-16}	9.7	0.78	4.78	19.4
WI F 13_2	1.164	0.49	1.52×10^{-16}	12.5	0.72	5.14	19.5
WI F 14	1.115	0.51	2.82×10^{-15}	4.8	0.38	4.68	17.8
WI 20_D	2.383	0.13	1.38×10^{-14}	71.7	2.96*	4.79	18.4
WI 21_A	1.546	0.37	3.09×10^{-15}	25.6	0.19	4.74	17.9
WI 21_C	1.410	0.44	1.8×10^{-16}	12.4	0.27	4.55	17.8
WI 21_D	1.511	0.38	6.27×10^{-16}	23.3	0.30	4.94	18.4
WI 21_H	1.363	0.46	1.3×10^{-16}	16.4	0.22	4.82	18.2
WI 22_B	1.148	0.51	2.29×10^{-15}	4.3	0.35	4.76	18.6
WI 23_B	1.343	0.45	1.22×10^{-16}	8.2	0.65	4.61	18.1
WI 24_B	1.144	0.52	2.03×10^{-14}	5.1	0.22	5.07	19
WI F 25_1	0.898	0.61	3.81×10^{-13}	3.1	0.53	5.71	19.2
WI F 34_2	1.124	0.51	3.52×10^{-14}	6.5	0.22	4.28	19.1
WI F 34_3	1.134	0.52	4.44×10^{-13}	5.5	0.24	3.88	19.8
WI F 35_2	1.189	0.49	3.76×10^{-14}	4.5	0.24	4.42	18.2
WI F 37_2	1.379	0.64	1.08×10^{-14}	6.8	5.07*	2.22	19.7
WI F 42_2	1.200	0.49	6.26×10^{-14}	4.6	0.43	3.44	19.7
WI F 44_1	0.911	0.59	4.74×10^{-13}	1.8	0.48	4.46	19.8
WI F 44_3	1.059	0.54	2.59×10^{-13}	2.5	0.40	4.64	20.2
WI F 46_1	0.803	0.66	2.73×10^{-13}	1.3	1.02	5.45	20.3
WI F 46_2	0.825	0.65	3.87×10^{-13}	2.0	1.15*	5.93	20.5
WI F 48	1.001	0.57	5.77×10^{-13}	2.8	0.48	5.66	20.2
WI F 52_1	1.493	0.40	2.4×10^{-16}	30.1	1.02*	5.74	20.1
WI F 52_2	1.506	0.38	8.02×10^{-16}	35.6	0.72	5.82	20.3
WI F 52_3	1.498	0.39	9.4×10^{-16}	32.7	0.56	5.78	22.6
WI F 54_2	1.474	0.38	5.85×10^{-15}	13.9	0.35	5.40	22.5
WI F 55_2	1.242	0.47	1.26×10^{-12}	10.0	0.16	4.94	22.5
WI F 56_1	1.107	0.49	1.48×10^{-13}	2.8	0.30	5.61	15.6
WI F 59	0.827	0.67	1.12×10^{-13}	1.9	0.62	5.5	19.1
WI F 60_2	1.191	0.47	2.95×10^{-15}	21.8	0.32	4.2	19.2
WI F 63_1	1.202	0.50	4.51×10^{-15}	7.4	0.35	4.7	19.4
WI F 63_2	1.225	0.50	5.03×10^{-15}	9.3	0.50	4.8	19.3
WI F 65	1.206	0.50	1.29×10^{-12}	7.9	0.42	4.7	19.7
WI F 67_2	1.086	0.55	6.55×10^{-13}	4.8	0.18	4.2	19.5
WI F 67_3	1.086	0.55	7.09×10^{-13}	5.2	0.39	4.1	19.5
WI F 70_2	1.225	0.50	6.26×10^{-13}	9.3	0.30	4.6	19.2
WI F 70_3	1.201	0.51	1.11×10^{-12}	8.6	0.27	5.3	19.2
WI F 73	1.264	0.49	3.6×10^{-14}	9.2	0.51	5.2	19.6
WI F 74	0.967	0.60	1.51×10^{-12}	2.0	0.24	5.3	19.4
WI F 78_2	1.175	0.52	4.09×10^{-15}	8.0	0.59	5.72	14.6
WI F 79_1	1.067	0.56	2.66×10^{-13}	9.5	0.70	3.76	14.6
WI F 90_1	1.467	0.45	2.66×10^{-13}	13.6	0.43	4.34	15
WI F 95_1	1.559	0.38	7.38×10^{-14}	26.4	1.38*	4.89	14.9
WI F 96_1	1.000	0.63	5.77×10^{-13}	7.4	0.32	5.38	15.6
WI F 105_1	1.894	0.18	1.11×10^{-14}	37.4	0.77	5.14	15.2
WI F 110_2	1.474	0.44	2.85×10^{-16}	24.4	0.43	3.42	15.4
WI F 110_3	1.531	0.42	6.82×10^{-17}	36.6	0.54	4.24	14.1
WI F 111_2	1.260	0.51	3.34×10^{-13}	6.3	0.35	3.87	15.7
WI F 112_2	1.505	0.42	4.68×10^{-16}	33.5	0.83	4.93	15.7
WI F 112_3	1.445	0.44	4.3×10^{-16}	23.3	1.49*	5.32	15.7
WI F 114	2.082	0.07	7.94×10^{-17}	111.9	0.83	4.98	15.8
WI F 115_2	1.145	0.55	1.4×10^{-16}	13.9	0.52	4.71	16.3
WI F 116_2	1.711	0.49	2.78×10^{-13}	3.7	0.30	3.08	16.5
WI F 116_3	2.140	0.39	1.77×10^{-14}	14.8	0.26	3.07	16.7
WI 30_1	1.564	0.33	1.57×10^{-13}	9.7	1.58*	4.49	17.7
WI 30_2	1.579	0.33	1.37×10^{-13}	9.6	1.21*	4.10	17.6
WI 30_3	1.658	0.30	4.93×10^{-13}	9.1	1.21*	4.14	17.6
WI 30_4	1.828	0.24	9.93×10^{-14}	7.3	1.67*	4.51	17.9

properties, as discussed in the introduction, are important for models of outgassing (e.g., Collinson and Neuberg, 2012; Chevalier et al., 2017), hydrothermal models (e.g., Todesco et al., 2010; Chiodini et al., 2010; Fournier and Chardot, 2012), and flank and dome stability models (e.g., Watters et al., 2000; Finn et al., 2001; Reid et al., 2001; John et al., 2008; Harnett et al., 2018; Peruzzetto et al., 2019).

It is important to now increase the number of samples to fine-tune the analyses presented, including samples that show deceases in porosity due to hydrothermal alteration (i.e., net dissolution). Hydrothermal alteration can increase (precipitation) or decrease (dissolution) the porosity of volcanic rocks, depending on factors such as the initial properties of the rock (e.g., rock type, crystal content, porosity, permeability),

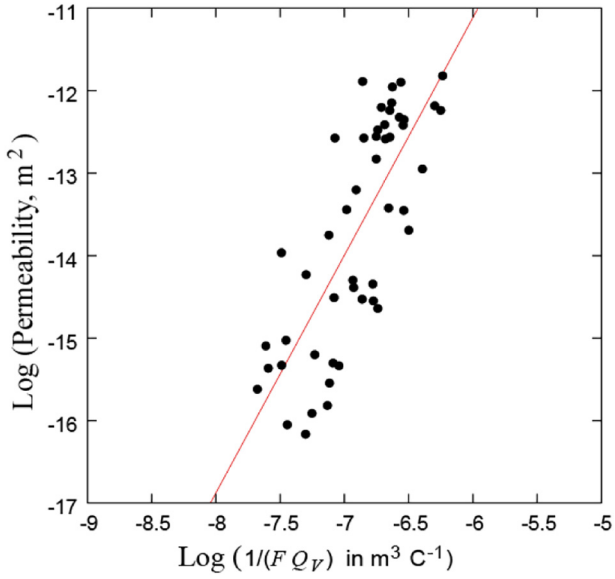

Fig. 7. Permeability as a function of alteration indicator (see text for details) for the rock samples from Whakaari (New Zealand). The solid line corresponds to the fit discussed in the main text. The coefficient of correlation is $R^2 = 0.60$. The fitted parameters are discussed in the main text.

the properties of the fluid (e.g., fluid composition, pH, temperature), and the pressure/depth (e.g., Browne, 1978). We present here data for rocks that experienced porosity loss resulting from mineral precipitation. An interesting avenue for future research would be therefore to provide data for rocks that experienced porosity increase as a result of dissolution to test Eqs. (2) and (3). For example, exposure to acid-sulfate fluids increased the porosity and permeability of volcanic rocks from the Solfatara region of Italy (Mayer et al., 2016) and increased the porosity and permeability and decreased the strength of andesite from Mt. Ruapehu (New Zealand) (Farquharson et al., 2019).

In summary, we show that the permeability and uniaxial compressive strength of volcanic rocks can be determined from an alteration index built from their porosity and CEC. This index can be built from induced polarization data and can therefore be mapped in 3D for a volcanic edifice. This opens exciting new perspectives for using geophysical data to compute an index for volcano outgassing and flank instability.

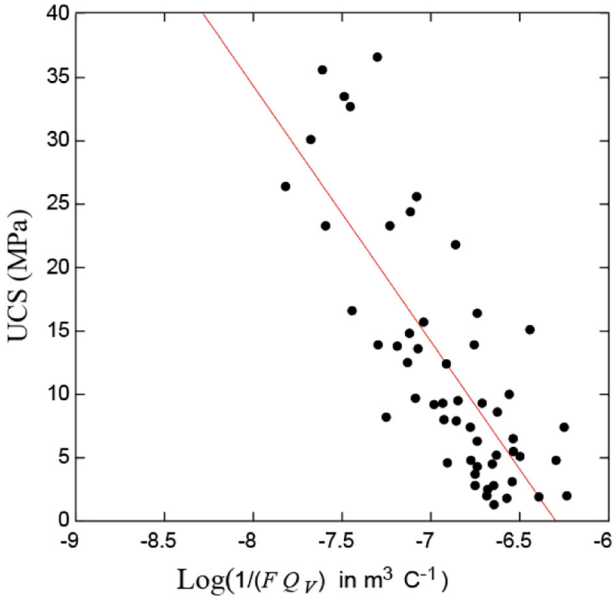

Fig. 8. Uniaxial compressive strength (UCS) as a function of alteration indicator (see text for details) for the rock samples from Whakaari (New Zealand). The solid line corresponds to the fit discussed in the main text. The coefficient of correlation is $R^2 = 0.61$. The fitted parameters are discussed in the main text.

CRediT authorship contribution statement

André Revil: Methodology, Writing - original draft, Conceptualization, Formal analysis, Methodology, Data curation, Supervision.**Antoine Coperey:**Investigation.**Michael J. Heap:**Methodology, Writing - original draft, Project administration.**Lucille Carbillet:**Investigation.

Declaration of competing interest

The authors declare that they have no known competing financial interests or personal relationships that could have appeared to influence the work reported in this paper.

Acknowledgments

The data used in this manuscript are available in Tables 1 and 2. The experimental materials were collected in 2016 and shipped to Strasbourg thanks to a Hubert Curien Partnership (PHC) Dumont d'Urville grant (number 31950RK). The authors are indebted to PeeJay Tours, Ben Kennedy, and Paul Siratovich for their help with sample collection. We thank Alessandro Aiuppa and two anonymous reviewers for their constructive comments regarding this manuscript.

References

Al-Harthi, A.A., Al-Amri, R.M., Shehata, W.M., 1999. The porosity and engineering properties of vesicular basalt in Saudi Arabia. Eng. Geol. 54 (3–4), 313–320.
Aran, D., Maul, A., Masfaraud, J.-F., 2008. A spectrophotometric measurement of soil cation exchange capacity based on cobaltihexamine chloride absorbance. Compt. Rendus Geosci. 340 (12), 865–871. https://doi.org/10.1016/j.crte.2008.07.015.
Archie, G.E., 1942. The electrical resistivity log as an aid in determining some reservoir characteristics. Pet. Trans. AIME 146, 54–62.
Browne, P.R.L., 1978. Hydrothermal alteration in active geothermal fields. Annu. Rev. Earth Planet. Sci. 6 (1), 229–248.
Cassidy, M., Manga, M., Cashman, K., Bachmann, O., 2018. Controls on explosive-effusive volcanic eruption styles. Nat. Commun. 9 (1), 2839.
Chevalier, L., Collombet, M., Pinel, V., 2017. Temporal evolution of magma flow and degassing conditions during dome growth, insights from 2D numerical modeling. J. Volcanol. Geotherm. Res. 333, 116–133.
Chiodini, G., Caliro, S., Cardellini, C., Granieri, D., Avino, R., Baldini, A., ... Minopoli, C., 2010. Long-term variations of the Campi Flegrei, Italy, volcanic system as revealed by the monitoring of hydrothermal activity. Journal of Geophysical Research: Solid Earth (B3), 115.
Ciesielski, H., Sterckeman, T., Santerne, M., Willery, J.P., 1997. Determination of cation exchange capacity and exchangeable cations in soils by means of cobalt hexamine trichloride. Effects of experimental conditions. Agronomie-Sciences des Productions Végétales et de l'Environnement 17 (1), 1–8.
Coats, R., Kendrick, J.E., Wallace, P.A., Miwa, T., Hornby, A.J., Ashworth, J.D., Lavallée, Y., 2018. Failure criteria for porous dome rocks and lavas: a study of Mt. Unzen, Japan. Solid Earth 9 (6), 1299–1328.
Collinson, A.S.D., Neuberg, J.W., 2012. Gas storage, transport and pressure changes in an evolving permeable volcanic edifice. J. Volcanol. Geotherm. Res. 243, 1–13.
Eichelberger, J.C., Carrigan, C.R., Westrich, H.R., Price, R.H., 1986. Non-explosive silicic volcanism. Nature 323 (6089), 598.
Farquharson, J., Heap, M.J., Varley, N.R., Baud, P., Reuschlé, T., 2015. Permeability and porosity relationships of edifice-forming andesites: a combined field and laboratory study. J. Volcanol. Geotherm. Res. 297, 52–68.
Farquharson, J.I., Wadsworth, F.B., Heap, M.J., Baud, P., 2017. Time-dependent permeability evolution in compacting volcanic fracture systems and implications for gas overpressure. J. Volcanol. Geotherm. Res. 339, 81–97.
Farquharson, J.I., Wild, B., Kushnir, A.R., Heap, M.J., Baud, P., Kennedy, B., 2019. Acid-induced dissolution of andesite: evolution of permeability and strength. Journal of Geophysical Research: Solid Earth 124 (1), 257–273.
Finn, C.A., Sisson, T.W., Deszcz-Pan, M., 2001. Aerogeophysical measurements of collapse-prone hydrothermally altered zones at Mount Rainier volcano. Nature 409 (6820), 600.
Fournier, N., Chardot, L., 2012. Understanding volcano hydrothermal unrest from geodetic observations: Insights from numerical modeling and application to White Island volcano, New Zealand. Journal of Geophysical Research: Solid Earth 117 (B11).
Frolova, J., Ladygin, V., Rychagov, S., Zukhubaya, D., 2014. Effects of hydrothermal alterations on physical and mechanical properties of rocks in the Kuril–Kamchatka island arc. Eng. Geol. 183, 80–95.

Ghorbani, A., Revil, A., Coperey, A., Soueid Ahmed, A., Roque, S., Heap, M.J., et al., 2018. Complex conductivity of volcanic rocks and the geophysical mapping of alteration in volcanoes. J. Volcanol. Geotherm. Res. 357, 106–127. https://doi.org/10.1016/j.jvolgeores.2018.04.014.

Giggenbach, W.F., Shinohara, H., Kusakabe, M., Ohba, T., 2003. Formation of acid volcanic brines through interaction of magmatic gases, seawater, and rock within the White Island volcanic-hydrothermal system, New Zealand. Spec. Publ. Soc. Econ. Geol. 10, 19–40.

Goode, P.A., Sen, P.N., 1988. Charge density and permeability in claybearing sandstones. Geophysics 53, 610–612.

Harnett, C.E., Thomas, M.E., Purvance, M.D., Neuberg, J., 2018. Using a discrete element approach to model lava dome emplacement and collapse. J. Volcanol. Geotherm. Res. 359, 68–77.

Heap, M.J., Kennedy, B.M., 2016. Exploring the scale-dependent permeability of fractured andesite. Earth Planet. Sci. Lett. 447, 139–150.

Heap, M.J., Xu, T., Chen, C.F., 2014. The influence of porosity and vesicle size on the brittle strength of volcanic rocks and magma. Bull. Volcanol. 76 (9), 856.

Heap, M.J., Kennedy, B.M., Pernin, N., Jacquemard, L., Baud, P., Farquharson, J.I., Mayer, K., 2015. Mechanical behaviour and failure modes in the Whakaari (White Island volcano) hydrothermal system, New Zealand. J. Volcanol. Geotherm. Res. 295, 26–42.

Heap, M.J., Kennedy, B.M., Farquharson, J.I., Ashworth, J., Mayer, K., Letham-Brake, M., Siratovich, P., 2017. A multidisciplinary approach to quantify the permeability of the Whakaari/White Island volcanic hydrothermal system (Taupo Volcanic Zone, New Zealand). J. Volcanol. Geotherm. Res. 332, 88–108.

Heap, M.J., Troll, V.R., Kushnir, A.R., Gilg, H.A., Collinson, A.S., Deegan, F.M., ... Walter, T.R., 2019. Hydrothermal alteration of andesitic lava domes can lead to explosive volcanic behaviour. Nature Communications 10 (1), 1–10.

Heap, M.J., Gravley, D.M., Kennedy, B.M., Gilg, H.A., Bertolett, E., Barker, S.L., 2020. Quantifying the role of hydrothermal alteration in creating geothermal and epithermal mineral resources: the Ohakuri ignimbrite (Taupō Volcanic Zone, New Zealand). J. Volcanol. Geotherm. Res. 390, 106703.

John, D.A., Sisson, T.W., Breit, G.N., Rye, R.O., Vallance, J.W., 2008. Characteristics, extent and origin of hydrothermal alteration at Mount Rainier Volcano, Cascades Arc, USA: implications for debris-flow hazards and mineral deposits. J. Volcanol. Geotherm. Res. 175 (3), 289–314.

Kennedy, B.M., Farquhar, A., Hilderman, R., Villeneuve, M.C., Heap, M.J., Mordensky, S., Reuschlé, T., 2020. Pressure controlled permeability in a conduit filled with fractured hydrothermal breccia reconstructed from ballistics from Whakaari (White Island), New Zealand. Geosciences 10 (4), 138.

Mayer, K., Scheu, B., Montanaro, C., Yilmaz, T.I., Isaia, R., Aßbichler, D., Dingwell, D.B., 2016. Hydrothermal alteration of surficial rocks at Solfatara (Campi Flegrei): petrophysical properties and implications for phreatic eruption processes. J. Volcanol. Geotherm. Res. 320, 128–143.

McGuire, W.J., 1996. Volcano instability: a review of contemporary themes. Geol. Soc. Lond., Spec. Publ. 110 (1), 1–23.

Moon, V., Bradshaw, J., de Lange, W., 2009. Geomorphic development of White Island Volcano based on slope stability modelling. Eng. Geol. 104, 16–30.

Moore, G.A., Agriculture Western Australia, National Landcare Program (W.A.), 1998. Soilguide: A Handbook for Understanding and Managing Agricultural Soils. Agriculture Western Australia, South Perth, W.A.

Mordensky, S.P., Villeneuve, M.C., Kennedy, B.M., Heap, M.J., Gravley, D.M., Farquharson, J.I., Reuschlé, T., 2018. Physical and mechanical property relationships of a shallow intrusion and volcanic host rock, Pinnacle Ridge, Mt. Ruapehu, New Zealand. J. Volcanol. Geotherm. Res. 359, 1–20.

Mordensky, S.P., Heap, M.J., Kennedy, B.M., Gilg, H.A., Villeneuve, M.C., Farquharson, J.I., Gravley, D.M., 2019. Influence of alteration on the mechanical behaviour and failure mode of andesite: implications for shallow seismicity and volcano monitoring. Bull. Volcanol. 81 (8), 44.

Mueller, S., Melnik, O., Spieler, O., Scheu, B., Dingwell, D.B., 2005. Permeability and degassing of dome lavas undergoing rapid decompression: an experimental determination. Bull. Volcanol. 67 (6), 526–538.

Mueller, S., Scheu, B., Spieler, O., Dingwell, D.B., 2008. Permeability control on magma fragmentation. Geology 36 (5), 399–402.

Okay, G., Leroy, P., Ghorbani, A., Cosenza, P., Camerlynck, C., Cabrera, J., Florsch, N., Revil, A., 2014. Spectral induced polarization of clay-sand mixtures: experiments and modeling. Geophysics 79, E353–E375.

Peruzzetto, M., Komorowski, J.C., Le Friant, A., Rosas-Carbajal, M., Mangeney, A., Legendre, Y., 2019. Modeling of partial dome collapse of La Soufrière of Guadeloupe volcano: implications for hazard assessment and monitoring. Sci. Rep. 9 (1), 1–15.

Pola, A., Crosta, G., Fusi, N., Barberini, V., Norini, G., 2012. Influence of alteration on physical properties of volcanic rocks. Tectonophysics 566, 67–86.

Reid, M.E., Sisson, T.W., Brien, D.L., 2001. Volcano collapse promoted by hydrothermal alteration and edifice shape, Mount Rainier, Washington. Geology 29 (9), 779–782.

Revil, A., Coperey, A., Shao, Z., Florsch, N., Fabricius, I.L., Deng, Y., et al., 2017a. Complex conductivity of soils. Water Resour. Res. 53 (8), 7121–7147. https://doi.org/10.1002/2017WR020655.

Revil, A., Le Breton, M., Niu, Q., Wallin, E., Haskins, E., Thomas, D.M., 2017b. Induced polarization of volcanic rocks. 1. Surface versus quadrature conductivity. Geophys. J. Int. 208, 826–844. https://doi.org/10.1093/gji/ggw444.

Revil, A., Qi, Y., Ghorbani, A., Coperey, A., Ahmed, A.S., Finizola, A., Ricci, T., 2019. Induced polarization of volcanic rocks. 3. Imaging clay cap properties in geothermal fields. Geophys. J. Int. https://doi.org/10.1093/gji/ggz207.

Rosas-Carbajal, M., Komorowski, J.C., Nicollin, F., Gibert, D., 2016. Volcano electrical tomography unveils edifice collapse hazard linked to hydrothermal system structure and dynamics. Sci. Rep. 6, 29899.

Saar, M.O., Manga, M., 1999. Permeability-porosity relationship in vesicular basalts. Geophys. Res. Lett. 26 (1), 111–114.

Schaefer, L.N., Kendrick, J.E., Oommen, T., Lavallée, Y., Chigna, G., 2015. Geomechanical rock properties of a basaltic volcano. Front. Earth Sci. 3, 29.

Sen, P.N., Straley, C., Kenyon, W.E., Whittingham, M.S., 1990. Surface-to-volume ratio, charge density, nuclear magnetic relaxation, and permeability in clay-bearing sandstones. Geophysics 55 (1), 61–69.

Sruoga, P., Rubinstein, N., Hinterwimmer, G., 2004. Porosity and permeability in volcanic rocks: a case study on the Serie Tobífera, South Patagonia, Argentina. Journal of Volcanology and Geothermal Research 132 (1), 31–43.

Todesco, M., Rinaldi, A.P., Bonafede, M., 2010. Modeling of unrest signals in heterogeneous hydrothermal systems. Journal of Geophysical Research: Solid Earth 115 (B9).

Vinegar, H.J., Waxman, M.H., 1984. Induced polarization of shaly sands. Geophysics 49, 1267–1287. https://doi.org/10.1190/1.1441755.

Voight, B., 2000. Structural stability of andesite volcanoes and lava domes. Philos. Trans. R. Soc. London, Ser. A 358 (1770), 1663–1703.

Wadsworth, F.B., Vasseur, J., Scheu, B., Kendrick, J.E., Lavallée, Y., Dingwell, D.B., 2016. Universal scaling of fluid permeability during volcanic welding and sediment diagenesis. Geology 44 (3), 219–222.

Watters, R.J., Zimbelman, D.R., Bowman, S.D., Crowley, J.K., 2000. Rock mass strength assessment and significance to edifice stability, Mount Rainier and Mount Hood, Cascade Range volcanoes. Pure Appl. Geophys. 157 (6–8), 957–976.

Waxman, M.H., Smits, L.J.M., 1968. Electrical conductivities in oil bearing shaly sands. Soc. Pet. Eng. J. 243, 107–122. https://doi.org/10.2118/1863-A.

Wyering, L.D., Villeneuve, M.C., Wallis, I.C., Siratovich, P.A., Kennedy, B.M., Gravley, D.M., Cant, J.L., 2014. Mechanical and physical properties of hydrothermally altered rocks, Taupo Volcanic Zone, New Zealand. J. Volcanol. Geotherm. Res. 288, 76–93.

Zimbelman, D.R., Rye, R.O., Breit, G.N., 2005. Origin of secondary sulfate minerals on active andesitic stratovolcanoes. Chem. Geol. 215 (1–4), 37–60.